L&O:F&E Advance Publication, published on February 11, 2011 as DOI:10.1215/21573698-1152081

Limnology and Oceanography
FLUIDS & ENVIRONMENTS

ORIGINAL ARTICLE

Interactions between the mat-forming alga *Didymosphenia geminata* and its hydrodynamic environment

Scott T. Larned,[1] **Aaron I. Packman,**[2] **David R. Plew,**[1] **and Kay Vopel**[3]

Abstract

Benthic autotrophs in oligotrophic rivers must adapt to and modify their hydrodynamic environment to balance the conflicting requirements of minimal drag (to minimize detachment risks) and maximal exposure to turbulent flow (to maximize nutrient acquisition). We explored flow–organism interactions using the benthic, freshwater alga Didymosphenia geminata. D. geminata *forms large mats in swift, oligotrophic alluvial rivers. The physical properties that allow* D. geminata *to resist detachment and proliferate under these harsh conditions are unknown. We transplanted cobbles with attached* D. geminata *mats from a riverbed to a flume and used velocimetry and microelectrode profiling to measure hydrodynamic and transport conditions above and within the mats over a wide range of flows. We then removed the mats from the cobbles and repeated the velocimetry measurements. Experiment results indicated that* D. geminata *mats reduce form-induced stresses and near-bed turbulent velocity fluctuations, which may reduce the risk of detachment.* D. geminata *mats also increase turbulent shear stress just above mat surfaces, which may enhance water column–mat solute exchange. High friction associated with flow at mat surfaces leads to very low velocities and predominantly diffusive transport within mats, which may in turn favor the retention of solutes derived from organic matter within and below mats. Enhanced mass transfer at mat surfaces and effective solute retention in mat matrices suggest a mechanism by which* D. geminata *cells acquire nutrients from different sources: advection-dominated transport of water-column nutrients to cells at mat surfaces, and diffusion-dominated transport from decomposing organic matter within mats, with minimal advective losses.*

Keywords: algal mat, river, shear stress, solute transport, turbulent flow

[1]National Institute of Water and Atmospheric Research, Christchurch 8011, New Zealand

[2]Department of Civil and Environmental Engineering, Northwestern University, Evanston, Illinois 60201, USA

[3]National Institute of Water and Atmospheric Research, Hamilton 3216, New Zealand; current address: Earth and Oceanic Sciences Research Institute and School of Applied Sciences, Auckland University of Technology, Auckland 1142, New Zealand

Correspondence to Scott T. Larned, s.larned@niwa.co.nz

Introduction

[1] Swift, oligotrophic rivers are physically harsh environments for benthic autotrophs. These organisms must resist or reduce high drag forces while acquiring dissolved nutrients at rates sufficient for sustained growth (Biggs et al. 2005). The morphological traits and mechanical behaviors most frequently associated with drag reduction appear to be mutually exclusive with those that enhance nutrient acquisition in benthic autotrophs. Low stature (Biggs et al. 1998), high flexibility (Suren et al. 2000; Plew et al. 2008), aggregation into dense mats with low surface-to-volume ratios (Vitt and Glime 1984), and reconfiguration (e.g., streamlining, compression; O'Hare et al. 2007)

all serve to minimize drag forces. However, the same traits tend to reduce the efficiency of nutrient acquisition by maximizing submergence in viscous boundary layers, where advective transport is limited (Raven 1992; Larned et al. 2004). Traits that enhance nutrient acquisition in oligotrophic water include protrusion into turbulent flow (Larned et al. 2004), wide-spaced branching (Steinman et al. 1992; Rice and Schuepp 1995), and flapping (Stevens et al. 2003), yet these increase the risk of structural failure (Schutten and Davy 2000; Puijalon et al. 2005).

[2] Benthic autotrophs may reduce the constraints imposed by nutrient scarcity and drag by modifying near-bed hydrodynamic conditions in several ways. When benthic autotrophs increase bed roughness, nutrient acquisition may be enhanced through increased turbulent mixing (Nikora et al. 1998; Larned et al. 2004). When they reduce large-scale roughness by filling gaps between rocks or by inducing skimming flow, benthic autotrophs reduce form drag and shear stress (Nikora et al. 1997; Suren et al. 2000). When advective flow through mat and canopy matrices is reduced or eliminated, nutrient acquisition from benthic sources and trapped organic matter may be enhanced, and dissolved nutrient losses minimized (Larned 1998; Dodds 2003).

[3] Mats composed of the cells and stalks of the benthic diatom *Didymosphenia geminata* (Lyngbye) A. Schmid are a useful system for examining the effects of benthic autotrophs on hydrodynamic conditions. The mats consist of a thin surface layer of pigmented cells underlain by a thick layer of interwoven polysaccharide stalks, which anchor the cells to substrata (Fig. 1). *D. geminata* occurs in hundreds of rivers across its native range in Eurasia, and in North and South America and New Zealand, where it was inadvertently introduced (Kilroy et al. 2008; Blanco and Ector 2009; Kumar et al. 2009). Many of the sites inhabited by *D. geminata* are characterized by high free-stream velocities ($>0.5\,m\,s^{-1}$) and low nutrient concentrations (dissolved inorganic nitrogen $<0.5\,mg\,L^{-1}$, dissolved reactive and total phosphorous $<0.1\,mg\,L^{-1}$) (Kilroy et al. 2008; Whitton et al. 2009). Despite these harsh conditions, *D. geminata* mats can reach densities $>1000\,g$ ash-free dry weight m^{-2} and dominate the benthos in terms of cover and biomass (Kirkwood et al. 2007; Miller et al. 2009; Kilroy et al. 2009). *D. geminata* mats overgrow and kill native periphyton, and they are efficient traps for seston (Flöder and Kilroy 2009). As a result, mats are often underlain by and impregnated with nutrient-rich particulate organic matter (POM) (Whitton et al. 2009). *D. geminata* research programs are under way in several countries where the alga has proliferated in rivers; a common goal in these programs is to explain the growth and persistence of *D. geminata* mats under harsh physical conditions (Kilroy et al. 2008; Miller et al. 2009; Whitton et al. 2009).

Fig. 1 Lateral view of *D. geminata*–covered cobbles and oxygen microelectrode through a flume sidewall. The maximum diameter of the electrode is 8 mm. Dark brown areas are pigmented *D. geminata* cells; light brown areas are exposed *D. geminata* stalks; and green areas are epiphytic green algae.

[4] In this study, we used *D. geminata* mats from a swift, oligotrophic river to test two hypotheses about the effects of algal mats on near-bed hydrodynamics. The first hypothesis was that algal mats reduce turbulent shear stress, form-induced stress, wake turbulence, and turbulent energy, relative to bare cobble beds. These modifications would serve to reduce the risk of mat detachment. The second hypothesis was that high friction at mat surfaces reduces advective transport within mat matrices, which reduces the loss of dissolved nutrients.

Methods

Algal Mat Collection and Flume Setup

[5] Cobbles with attached *D. geminata* mats were collected from a 50-m reach in the lower Waitaki River, on

New Zealand's South Island, on two dates in February 2007; each collection was used for one experiment. The Waitaki is an alluvial river that flows from New Zealand's Southern Alps to the Pacific Ocean. The bed of the lower Waitaki is dominated by coarse graywacke substrata (boulders to fine gravels). *D. geminata* was introduced to the Waitaki River between 2004 and 2005, and by January 2006, the shallow littoral zone along >50 km of the lower Waitaki was partially covered by 1–5 cm thick *D. geminata* mats.

[6] *D. geminata*–covered cobbles were collected from channel margins at 0.2–0.5 m depth. Before removing the cobbles, freestream ($0.6 \times$ depth) and near-bed (5 cm above the bed) velocity measurements were made with an acoustic Doppler velocimeter (Flowtracker, Sontek/YSI Inc., USA). The free-stream velocity was 39 ± 17 cm s^{-1} (mean $\pm$ 1 SD; range: 13–86 cm s^{-1}), and the near-bed velocity was 14 ± 10 cm s^{-1} (range: 0–49 cm s^{-1}). Two hundred cobbles were collected on each date. The diameter of cobbles was 10.7 ± 2.5 cm (range: 3.1–22.0 cm).

[7] *D. geminata*–covered cobbles were transported from the river to the laboratory within 2 h, with frequent misting to minimize desiccation. In the laboratory, the cobbles were placed on a 5-cm thick layer of coarse river gravel, in a recirculating flume. The cobbles had the same orientation relative to flow direction that they had in the river. The flume was then filled with unchlorinated tap water, which was slowly recirculated until experimental runs started the following morning. With the cobbles in place, planar cover of *D. geminata* in the working section was $>90\%$; the remaining area consisted of exposed cobble edges and gaps between mats.

[8] The flume has a clear acrylic bed and sidewalls (6 m long, 0.6 m wide, 0.4 m high), a stainless steel return pipe equipped with a Veneroni E pump and impeller with a 2.4 kW motor (Veneroni LLC, Italy), a Teco 7300CV speed controller (TECO-Westinghouse Motor Co., USA), an ABB MagMaster electromagnetic flow meter (ABB Kent-Taylor Ltd., UK), and dual jacks at the downstream end to adjust the bed slope. A perforated plate in the return pipe and a 60-cm-long entry section with large, clean cobbles upstream of the working section were used to reduce the effects of turbulent fluctuations from the pump.

Experiment Procedures

[9] Two experiments were carried out, corresponding to the two collections of *D. geminata*–covered cobbles, and four to six runs were completed at different flow rates during each 4-day experiment. Hydrodynamic measurements were made at three different spatial scales during each run, including water surface slopes measured at the whole-channel scale to calculate friction coefficients; vertical velocity profiles measured at multiple points in the working section to characterize the structure of the overlying flow; and microelectrode profiles measured at multiple points above and within individual *D. geminata* mats to assess solute transport and mixing conditions. Electrical conductivity, pH, and temperature were measured continuously in the flume water with Knick meters and sensors (Knick Elektronische Messgeräte, Germany). During each experiment, several runs were completed with *D. geminata* mats in place; then the mats were removed from the cobbles without altering cobble positions. The flume was then drained, rinsed, and refilled to the same depth above the flume bed, and the whole-channel and velocity profile measurements were repeated with the bare cobbles. Hydraulic conditions in each experimental run are given in Appendix Tables A1 and A2.

Whole-Channel Measurements

[10] Flow depth (from water surface to *D. geminata* or bare cobble surface) was measured manually at the same 200 locations before and after *D. geminata* mats were removed, during both experiments. These data were used to calculate mean flow depth and mat thickness. Cross-sectional mean velocity (U_0) was calculated by dividing volumetric flow by the product of mean water depth and flume width. During the second experiment, whole-channel flow conditions in the presence and absence of *D. geminata* were characterized using the Darcy-Weisbach friction factor (f), calculated from measurements of water surface slope (S), which was measured with a manometer over a range of flow rates

($9–45\,L\,s^{-1}$) and flow depths (10–17 cm). For each measurement, the gradient of the flume was adjusted so that S was equal to the bed slope over the flume working section.

Velocity Profiles

[11] Detailed hydrodynamic measurements were made using acoustic Doppler velocimetry (ADV) and particle tracking velocimetry (PTV). ADV measurements were made with Sontek Micro-ADV Lab instruments (Sontek/YSI Inc., USA) at six mean velocities (U_0 range: 14.7–59.1 $cm\,s^{-1}$) with *D. geminata*–covered cobbles, and at four mean velocities (U_0 range: 13.0–38.5 $cm\,s^{-1}$) after *D. geminata* mats were removed (Table 1). A constant water depth (20 cm relative to the bottom of the flume) was used for all ADV measurements. The probes of three down-looking ADVs were attached to a mobile carriage mounted above the flume, in a row parallel to the flow and spaced 10 cm apart. The carriage has geared drives for positioning probes along the X (longitudinal), Y (transverse), and Z (vertical) axes with 1.0-mm accuracy on the X and Y axes and 0.5-mm accuracy on the Z axis. Velocities in each direction were measured in a 0.08-cm^3 sampling volume 5 cm below each probe. The locations of *D. geminata* mat or bare cobble surfaces were indicated by abrupt increases in the signal-to-noise ratio to >30 dB. The ADV sampling frequency was 25 Hz, the duration was 2 min, and the minimum signal-to-noise ratio was 15 dB. Sontek seeding material (hollow glass spheres, approx. 10 μm diameter) was used to improve ADV performance. ADV measurements were made at 10–13 vertical positions at 12 (experiment 1) or 24 (experiment 2) locations in the XY-plane during each run. An additional set of velocity measurements was made with 5-min sampling durations at each of 13 vertical positions, at three locations over the bed, with *D. geminata* mats in place and again after the mats were removed. The 5-min time series were used for analyses of velocity spectra, described below. A total of 1453 velocity time series were logged and post-processed with Sontek WinADV software. All ADV time series were checked for data spikes and noise during post-processing; only time series with $<2\%$ of the data identified as spikes or noise were retained for analyses.

[12] The ADVs provided time series of the three-dimensional (3D) velocity vector at each measurement location. The velocity vector was resolved into components in the X, Y, and Z directions (u, v, and w, respectively). The time average of each velocity component was calculated, denoted here as U, V, and W for the mean velocity in the X, Y, and Z directions, respectively. Reynolds stress was calculated as the covariance of the measured velocity fluctuations, for example, $-\overline{u'w'}$, $-\overline{u'v'}$, where the overbars indicate time-averaged quantities. Autospectra of longitudinal, transverse, and vertical velocity fluctuations (u', v', and w') were calculated with the data from the 5-min velocity time series. Spectra were smoothed using 256-point Hanning windows with 50% overlap (Bendat and Piersol 2000). Spectra were converted from frequency space to wavenumber space using the frozen turbulence approximation, $k = 2\pi f/U$, which requires that u'/U is small.

[13] Digital videography was used for PTV analyses in the XZ-plane, during a single experimental run (experiment 2, flow rate: $14\,L\,s^{-1}$). Image sequences were recorded in three parallel planes distributed across the width of the flume working section; each plane was 40 cm long and extended from the water surface to the flume bottom. Two image sequences were recorded at each location and combined to provide a total recording period of 80 s for each location and flow rate. At the start of the run, the flume was seeded with resin particles (Pliolite styrene resin, Eliokem, France) with

Table 1 Flow rates, cross-sectional mean velocities (U_0), and shear velocities (u_*) in flume experiments with *Didymosphenia geminata* mats and bare cobbles.

	Experiment	Flow ($L\,s^{-1}$)	U_0 ($cm\,s^{-1}$)	u_* ($cm\,s^{-1}$)
D. geminata mats	1	14	14.7	1.4
	1	27	29.4	2.2
	1	40	43.6	4.4
	2	13.5*	—	—
	2	20	23.9	2.2
	2	35	41.8	4.2
	2	50	59.1	—
Bare cobbles	1	14	13.0	1.2
	1	27	26.0	1.9
	1	40	38.5	3.8
	2	13.5*	—	—
	2	35	35.0	3.9

* PTV measurements only.

a specific gravity of 1.03 and sieved to a diameter range of 90–125 μm. A light sheet was generated with a 2-kW halogen bulb in a ventilated box with a 6-mm slit. Image sequences of 1750 frames were recorded with a CV-M4 + CL monochrome digital camera (JAI, Denmark) at 43.5 Hz, at a resolution of 1380 × 515 pixels. The image sequences were analyzed using FluidStream 7.0 PTV software (Nokes 2007) in four steps. First, particle positions in each image frame were identified based on pixel intensity. Second, particles were matched between subsequent frames using a combination of best-match costing algorithms. Third, steps 1 and 2 were used to calculate particle velocities and trajectories, and these were projected onto (5 × 5 mm)-grids using a triangulation scheme to provide a time series of 2D velocity fields (Cline and Renka 1984). Fourth, the 2D velocity data from the three measurement locations were combined to calculate spatially averaged values of flow parameters.

[14] In contrast to the 3D ADV measurements, PTV measurements were limited to the longitudinal (u) and vertical (w) velocity components. However, the ADVs could not sample in the upper 50 mm of the water column, and the spacing between measurement points was greater than the PTV grids. For these reasons, PTV data were used rather than ADV data for assessing 2D flow characteristics. The mean velocity components U and W, Reynolds stresses $\overline{u'u'}$, $\overline{w'w'}$, $-\overline{u'w'}$, and partial turbulent kinetic energy (partial TKE) $K = 0.5(\overline{u'u' + w'w'})^{0.5}$ were calculated at each grid point in the PTV image frames. The term "partial" refers to the absence of the transverse velocity component v. We assumed that the transverse component was small relative to the longitudinal and vertical components; comparisons with ADV measurements indicated that the partial K underestimated total K by approximately 40%. Spatial averages of mean velocity and Reynolds stress were obtained by averaging all measurements at each height increment. Spatial averages are denoted with angular brackets, $\langle\ \rangle$. PTV data were also used to construct vertical profiles of the total shear stress τ_{xz}, which has three components in flow above rough beds: Reynolds stress $-\langle\overline{u'w'}\rangle$, form-induced stress $-\langle U'W'\rangle$ where U' and W' are the differences between the local time-averaged velocity and the spatially averaged velocity components, and viscous stress $\nu\frac{\partial\langle U\rangle}{\partial z}$, where ν is the kinematic viscosity (Nikora et al. 2001):

$$\frac{\tau_{xz}}{\rho} = -\langle\overline{u'w'}\rangle - \langle U'W'\rangle + \nu\frac{\partial\langle U\rangle}{\partial z}. \tag{1}$$

Note that shear stress is divided by water density ρ in equation (1).

[15] The rate of turbulence production P was also estimated from the PTV data. Neglecting transverse components, turbulence production is controlled by turbulent Reynolds and normal stresses:

$$P = -\overline{u'w'}\left(\frac{\partial U}{\partial z} + \frac{\partial W}{\partial x}\right) - \overline{u'u'}\left(\frac{\partial U}{\partial x}\right) - \overline{w'w'}\left(\frac{\partial W}{\partial z}\right) \tag{2}$$

Central differences were used to calculate the spatial derivatives. The high spatial resolution provided by PTV (5 × 5 mm) allowed us to map turbulence production rates and identify regions where turbulence was generated.

[16] Shear velocities (u_*) were calculated from velocity profiles using the universal velocity logarithmic law (i.e., law of the wall). For rough beds, this law is used in the form

$$\frac{\langle U\rangle}{u_*} = \frac{1}{\kappa}\ln\left(\frac{z-d}{z_0}\right), \tag{3}$$

where z is the elevation above the datum (the flume bed), d is the displacement height that defines the virtual origin of the logarithmic velocity profile, κ is von Karman's constant, and z_0 is the roughness length scale. We used u_* based on velocity profiles in lieu of u_* based on near-bed turbulent stress (e.g., Nikora et al. 1998) for three reasons: u_* estimated from turbulent stress neglects the contribution of the form-induced stresses; more data points were available from velocity profiles than from near-bed turbulent shear stress measurements; and there was greater measurement error for turbulent shear stresses than for mean velocities. However, to obtain u_* from equation (3) first required an estimate of d (the roughness length scale is not required as u_*/κ is calculated from the slope of $\langle U\rangle$ versus $\ln(z-d)$). We used PTV data from run 2 to calculate the displacement

height with and without *D. geminata* mats, by rearranging equation (3) to give

$$z = z_0 \exp\left(\frac{\kappa\langle U\rangle}{u_*}\right) + d. \quad (4)$$

Values of d and z_0 were obtained by linear regression of z against $\exp(\kappa\langle U\rangle/u_*)$ from the spatially averaged PTV data. The shear velocity in equation (4) was estimated by extrapolating the turbulent shear stresses from near the surface (where $-\langle U'W'\rangle$ is negligible) to the bed.

Microelectrode Measurements

[17] To characterize the solute transport environment within and above *D. geminata* mats, we measured vertical profiles of hydrogen transport and dissolved oxygen concentration with microelectrodes. Hydrogen transport was measured with a microsensor equipped with an internal hydrogen reservoir and diffusion barrier (Revsbech et al. 1998). Hydrogen transport due to molecular diffusion alone was defined as the electrode signal when the sensor was held in stagnant water (flume pump turned off). Subsequent profiles measured in flowing water were divided by the profiles measured in stagnant water to give normalized transport rates (hereafter, NT). NT approaches zero as advection predominates over diffusion.

[18] Oxygen concentration and NT profiles were measured above and within two topographic features that characterize *D. geminata* mats, small depressions, and flat "plateaus" (Fig. 1). This approach was based on previous observations that topographic features on algal mats influence boundary layer thickness and solute transport rates, and that the overall effect of rugose mat topography is to enhance solute transport (Jørgensen and Des Marais 1990; De Beer and Kühl 2001; Vopel and Hawes 2006).

[19] A motorized micromanipulator was used to position Unisense oxygen (model OX-50) and hydrogen (model H2-50) microelectrodes (Unisense A/S, Denmark). A Unisense PA2000 picoammeter polarized the microelectrodes and supplied the signals to a Unisense ADC 216 analog-digital converter. Unisense Profix data-acquisition software was used to control the micromanipulator and record microelectrode output. Downwelling photosynthetically active irradiance (E_d) was provided by 10 Osram Lumilux L 30W/840 cool white bulbs (Osram Ltd., UK) mounted 0.3 m above the water surface over the working section. During illuminated periods, E_d at the *D. geminata* mat was approximately 120 μmol quanta m^{-2} s^{-1}.

[20] Vertical NT profiles were measured above and within a plateau on two *D. geminata* mats located at opposite ends of the working section. At each mat, hydrogen electrode signals were recorded at 0.2-mm vertical increments, at each of five mean velocities ranging from 0 (pump turned off) to 59.1 cm s^{-1}. The individual profiles extended from 2 mm above to 6 mm below the mat surfaces. To prevent inserting the microelectrode into the hole created by a previous profile, the profiles at each mat were offset horizontally by several millimeters. The location of the mat surface in each profile was identified by an abrupt change in the slope of the electrode signal profile. Hydrogen electrode signals were converted to NT values as described above.

[21] Dissolved oxygen saturation was measured at 0.1-mm vertical increments above and within three depressions and three plateaus on one *D. geminata* mat. Three replicate measurements were made at each depression and plateau at three mean velocities (U_0: 14.7, 41.8, 43.6 cm s^{-1}) during light and dark periods. The profiles were spaced several millimeters apart horizontally to ensure that the probe was not inserted into a hole in the mat made during a previous profile. The oxygen microelectrode had an outside tip diameter of approximately 50 μm, a 90% response time of <1 s, a stirring sensitivity of $<2\%$, and a detection limit of 0.3 μmol L^{-1}. The microelectrode was calibrated in air-saturated water and in Na_2SO_3-deoxygenated water. Oxygen penetration depth (OPD) was estimated as the shallowest depth in a mat at which the dissolved oxygen concentration was below the detection limit.

Results

Whole-Channel Measurements

[22] During the two 4-day experiments, electrical conductivity ranged from 132 to 137 μS cm^{-1}, pH ranged from 7.6 to 7.7, and water temperature ranged from 17.6 to 19.8 °C. Friction coefficients were generally higher in

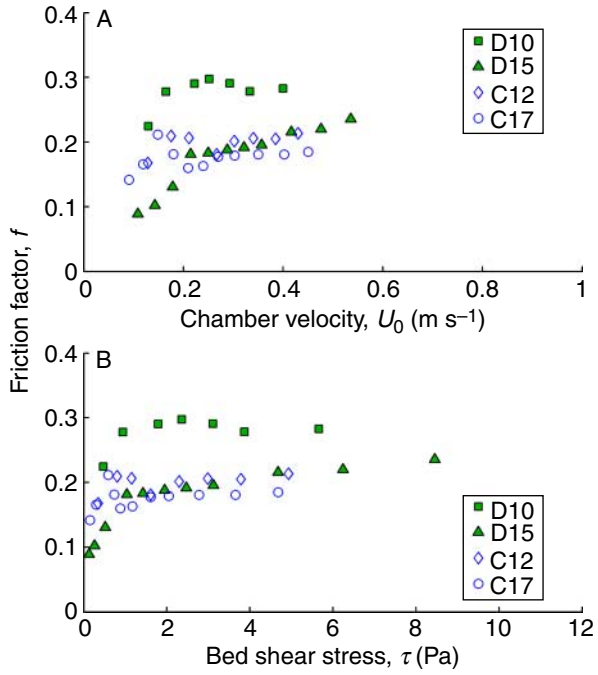

Fig. 2 Darcy-Weisbach friction factor as a function of cross-sectional mean velocity U_0 (top) and bed shear stress τ (bottom) at two water depths, with *D. geminata* mats (D) and over bare cobbles (C). For clarity, data from four runs in one experiment are shown. D10 and D15: experimental runs with *D. geminata* mats in place, and flow depths of 10 and 15 cm, respectively. C12 and C17: experimental runs with *D. geminata* mats removed, and flow depths of 12 and 17 cm, respectively.

the presence of *D. geminata* (0.22 ± 0.06) compared with bare cobbles (0.18 ± 0.02), indicating that *D. geminata* mats caused an increase in friction of approximately 20% (Fig. 2). The friction coefficient increased asymptotically with mean velocity (U_0) and with bed shear stress (τ) in the presence of *D. geminata* (Fig. 2). No effects of mean velocity or bed shear stress on friction coefficients were apparent after the *D. geminata* mats were removed, as expected for a fixed-bed morphology under fully rough turbulent flow.

Velocity Profiles

[23] ADV measurements were averaged across the *XY*-plane to obtain vertical profiles of mean downstream velocity ($\langle U \rangle$), Reynolds stress ($-\langle u'w' \rangle$), and turbulent kinetic energy ($-\langle K \rangle$) for each experimental run. Each parameter was normalized by cross-sectional mean velocity (U_0). Profiles of normalized mean velocity ($\langle U \rangle / U_0$) were logarithmic over the bare cobbles and the *D. geminata* mats (Fig. 3A, B). Velocity profiles over bare cobbles were very similar across flow rates and between experiments (Fig. 3A). Velocity profiles over *D. geminata* mats were similar close to the bed, and diverged toward the water surface (Fig. 3B). At most vertical positions, $\langle U \rangle / U_0$ decreased with increasing flow over the *D. geminata* mats, which may reflect compression of the mats at high flow rates, resulting in greater cross-sectional flow area. This compression was not accounted for when estimating U_0. Normalized Reynolds shear stress ($-\langle u'w' \rangle / U_0^2$) increased linearly with proximity to the bare cobble bed (Fig. 3C), but no clear linear or curvilinear pattern was evident in profiles of Reynolds stress above *D. geminata* mats (Fig. 3D). Relative turbulent kinetic energy also increased linearly with proximity to the bare cobble bed (Fig. 3E) but reached maximum values several centimeters above *D. geminata* mats (Fig. 3F). The average ratio of K/U_0^2 at the mean bed elevation was approximately 0.04 for bare cobbles and approximately 0.03 for *D. geminata* mats.

[24] Selected results of the autospectra analysis are shown in Fig. 4. The autospectra of vertical velocity fluctuations 20 mm above *D. geminata* mats were less energetic at low wave numbers (k) than those above bare cobbles. As low wave numbers correspond to large-eddy length scales, these results indicate that *D. geminata* reduces the energy of large turbulent eddies near mat surfaces. The autospectra of vertical velocity fluctuations 80 mm above *D. geminata* mats and bare cobbles were indistinguishable (Fig. 4). Similar patterns were seen in spectra of the u' and v' components (not shown).

[25] Unlike the ADV measurements, PTV measurements indicated that Reynolds ($-\langle u'w' \rangle / U_0^2$) and total shear stress (τ_{xz}) above *D. geminata* mats increased with proximity to the bed. The difference in results using ADV and PTV data may be due to the differences in total sampling volumes. After post-processing, 1–24 ADV measurements with individual sampling volumes of 0.08 cm^3 were averaged for each vertical interval; the total sampling volume represented by each point in Fig. 3 is 0.08–1.92 cm^3. In contrast, each data point in the PTV profiles shown in Fig. 5 represents a sampling volume of 36 cm^3.

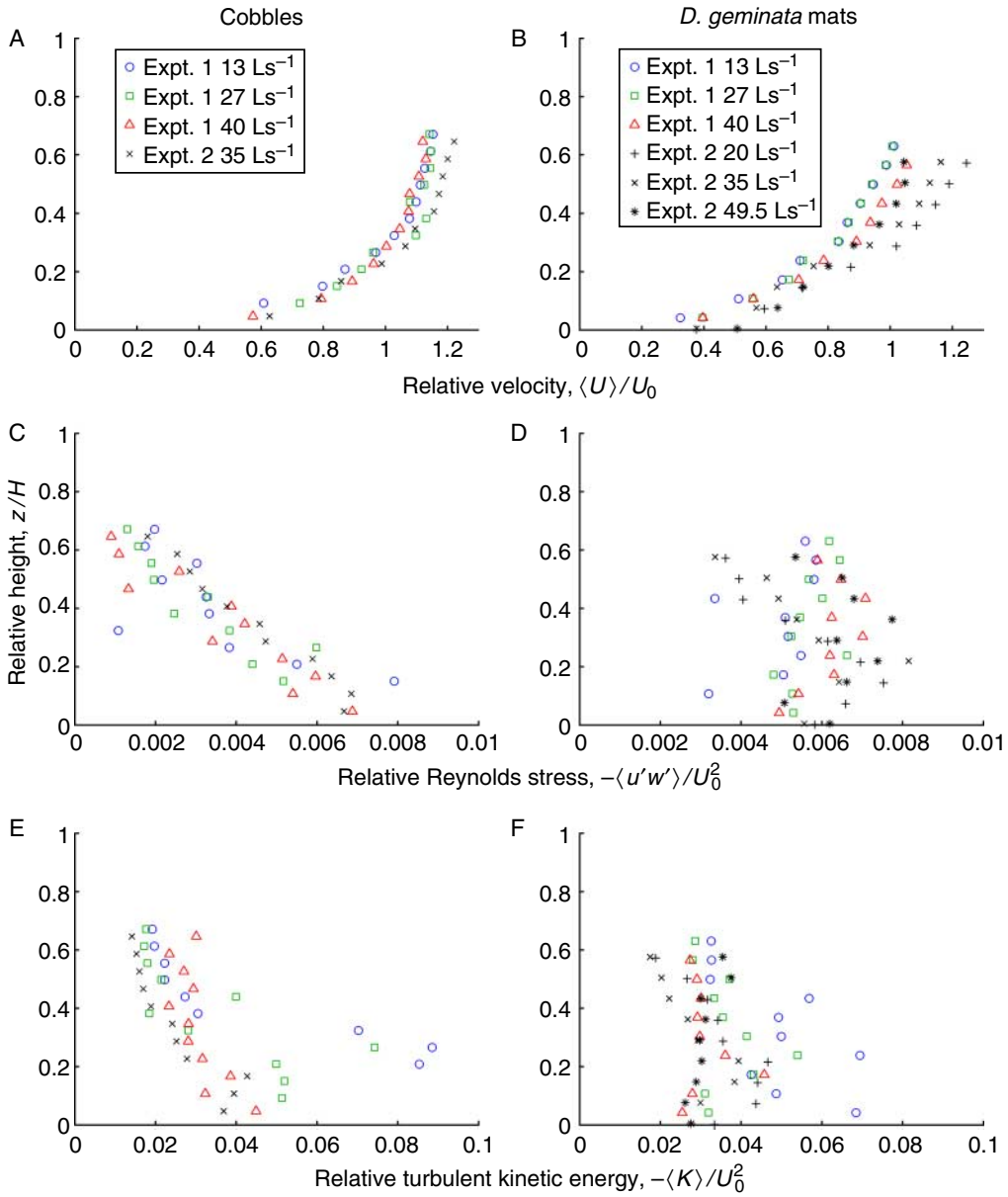

Fig. 3 Vertical profiles from ADV measurements at a range of volumetric flow rates, from experiments 1 and 2. Panels A and B: horizontally averaged mean longitudinal velocity $\langle U \rangle$ normalized by mean velocity U_0 over bare cobbles (A) and *D. geminata* mats (B). Panels C and D: mean Reynolds stress $-\langle u'w' \rangle$ normalized by U_0^2 over bare cobbles (C) and *D. geminata* mats (D). Panels E and F: mean turbulent kinetic energy $\langle K \rangle$ normalized by U_0^2 over bare cobbles (E) and *D. geminata* mats (F). Legend in A applies to C and E; legend in B applies to D and F. Vertical axes: height above the average bed elevation z, normalized by flow depth H to align profiles.

[26] Total shear stress immediately above *D. geminata* mats and bare cobbles was comparable, but Reynolds stress ($-\langle u'w' \rangle / u_*^2$) was greater above mats, and form-induced stress ($-\langle U'W' \rangle / u_*^2$) was greater above bare cobbles (Fig. 5). The region above the bed where form-induced stresses are prominent (i.e., the roughness layer) was similar in thickness above bare cobbles and *D. geminata* mats (approx. 40% of the flow depth) but was shifted upward above the mats (Fig. 5). Viscous stress ($\nu(\partial \langle U \rangle / \partial z) / u_*^2$) above mats and bare cobbles was negligible.

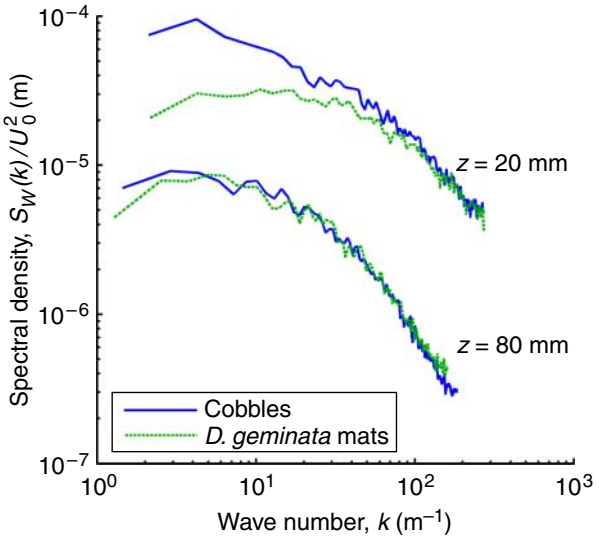

Fig. 4 Autospectra of fluctuations in vertical velocity w' at heights of 20 and 80 mm above bare cobbles and *D. geminata* mats in experiment 2, at a flow rate of 35.0 L s^{-1}. The spectra at 80 mm are shifted downward by 1 decade for clarity. Horizontal axis: wave number. Vertical axis: spectral energy density normalized by U_0^2.

[27] Displacement heights of −125.9 mm for the *D. geminata* mats, and −167.2 mm for the bare cobbles were calculated from the PTV data from experiment 2. For experiment 1, displacement heights were estimated using the differences in mean bed elevation in the two experiments. These displacement heights were substituted into equation (3) to calculate u_* from the ADV data (Table 1). Fluidization of *D. geminata* mat surfaces at the highest flow rate used (49.5 L s^{-1}) led to unreliable estimates of displacement heights, which precluded a calculation of u_* for this experimental run. Shear velocities increased with flow rate and with U_0 (Table 1). The ratio of u_*/U_0 increased with flow rate, which was consistent with the increase in friction factor (Fig. 2). On average, u_* at *D. geminata* mat surfaces was 13% higher than u_* at bare cobble surfaces.

Distributions of Turbulent Kinetic Energy, Turbulent Stresses, and Turbulence Production

[28] Partial turbulent kinetic energy K, Reynolds stress $-\overline{u'w'}$, and turbulence production rates P from a single XZ-plane are shown in Fig. 6. Compared to bare cobbles, K was generally higher above *D. geminata* mats. Higher K above *D. geminata* mats is partly due to the reduction in flow depth caused by the mats, which resulted in higher cross-sectional mean velocities at each flow rate (Table 1). However, maximum values of K/U_0^2 were still higher above the *D. geminata* mats than the bare cobbles, and K was maximal in the interfacial layer immediately above and between bare cobbles (Fig. 6A). In contrast, K was maximal several centimeters above *D. geminata* mat surfaces (Fig. 6B). As K is a measure

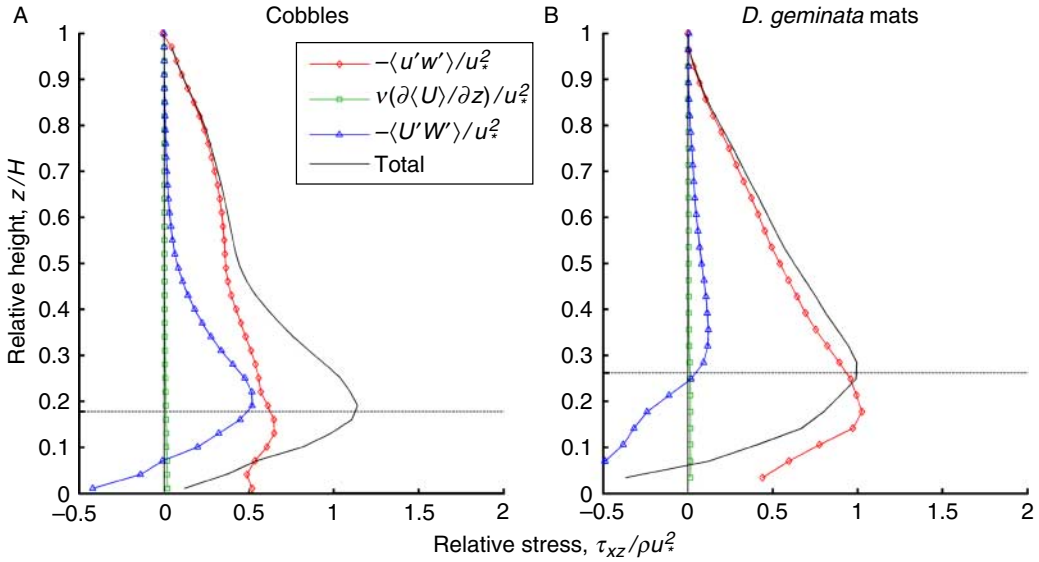

Fig. 5 Vertical profiles of the horizontally averaged components of shear stress τ_{xz} normalized by ρu_*^2 over bare cobbles (A) and *D. geminata* mats (B). Profiles are based on PTV data, at a flow rate of 13.5 L s^{-1}. Horizontal dotted line: maximum heights of cobbles and *D. geminata* mats. Vertical axes are as in Fig. 3.

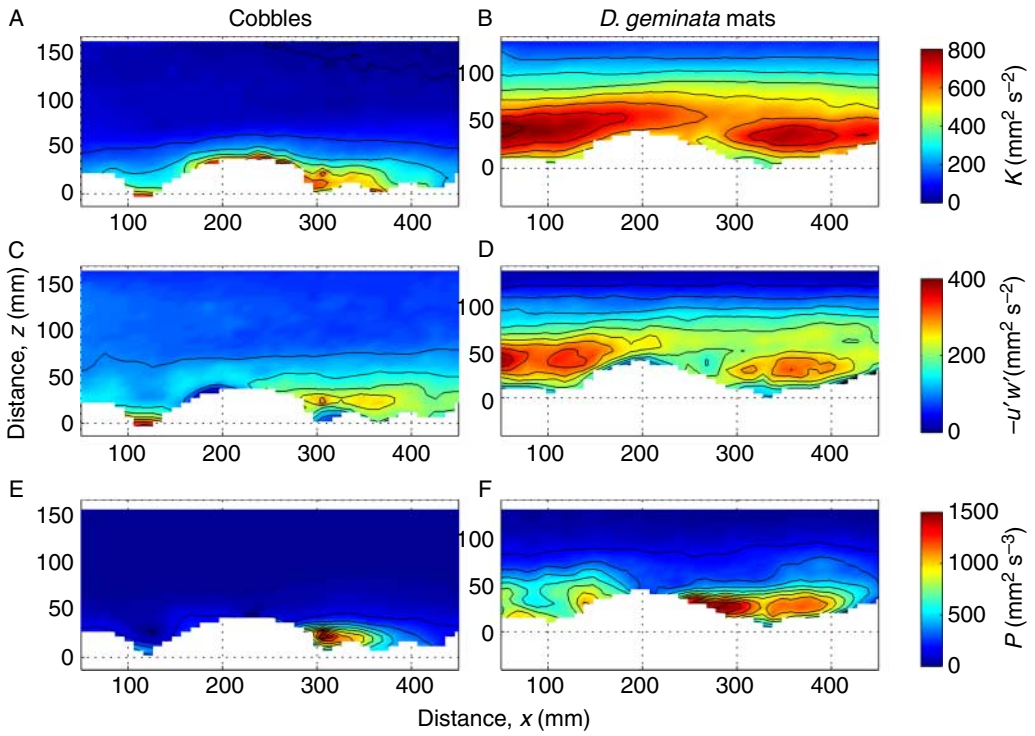

Fig. 6 Longitudinal distributions of partial turbulent kinetic energy K (A and B), Reynolds stress $-u'w'$ (C and D), and turbulence production rate P (E and F) over bare cobbles and *D. geminata* mats. Distributions are based on PTV data from experiment 2, at a flow rate of 13.5 L s^{-1}. Flow is from left to right, through the central 40 cm of the flume working section. Vertical axes: height above mean bed elevation.

of the magnitude of turbulent velocity fluctuations, relatively low K immediately above *D. geminata* mat surfaces indicates that near-bed velocity fluctuations were reduced in comparison to bare cobbles. Reynolds stress was highest in the interfacial layer of the bare cobble bed (Fig. 6C) and highest in the roughness layer over the *D. geminata* mats (Fig. 6D). These observations corroborate the spatially averaged stress profiles shown in Fig. 5. Stronger eddy shedding occurred behind bare cobbles (Fig. 6A and C) than *D. geminata* mats (Fig. 6B and D), resulting in greater turbulence and turbulent shear in the wakes of bare cobbles. The *D. geminata* mats reduced bed roughness by filling gaps between cobbles, which reduced flow separation and turbulence in the interfacial layer (Fig. 6B and D). For bare cobbles, P was highest in the wake of cobbles and generally low elsewhere (Fig. 6E). For *D. geminata* mats, P was highest in the wake of large bed forms and was shifted vertically above the bed compared with bare cobbles (Fig. 6F).

Solute Transport

[29] NT values within *D. geminata* mat matrices indicated that the transport environment >1 mm below mat surfaces was dominated by molecular diffusion at low-to-moderate mean velocities (<42 cm s^{-1}). At the highest mean velocity (59.1 cm s^{-1}), advective transport dominated, as indicated by partial fluidization of the upper 4–5 mm of the mat (Fig. 7). In the uppermost layers of *D. geminata* mats (<1 mm below the surface), transport was enhanced by advection at mean velocities ≥ 14.7 cm s^{-1} (Fig. 7). Data from the uppermost layers probably represent an average between overlying and internal transport conditions, due to volumetric averaging in hydrogen-transport measurements.

Oxygen Profiles

[30] During illuminated periods and at low-to-moderate mean velocities (14.7–29.4 cm s^{-1}), the surficial layer of the *D. geminata* mat and the water 1–2 mm above the mat surface were supersaturated with oxygen

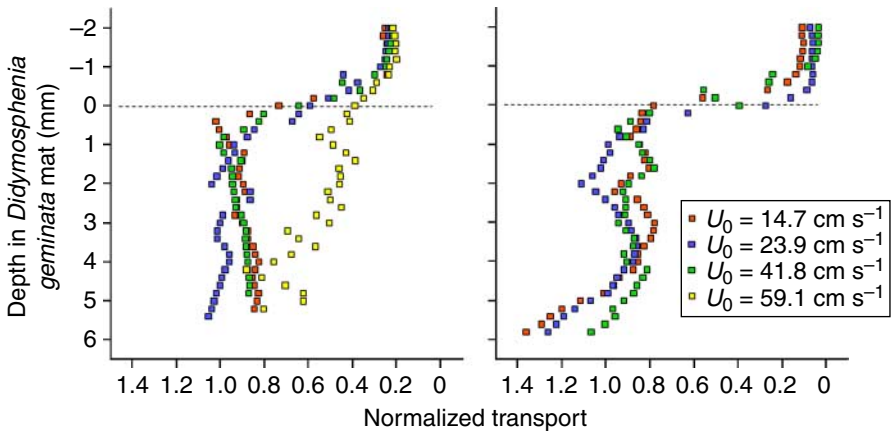

Fig. 7 Microprofiles of normalized solute transport measured with a hydrogen microsensor above and within plateau areas on *D. geminata* mats. The two panels correspond to two different *D. geminata* mats, with replicate profiles for each mat. Dashed lines indicate mat surfaces.

(Fig. 8A, B, D, E). The shapes of the oxygen profiles for low-to-moderate mean velocities indicate that oxygen produced by photosynthesis at the mat surface was transported into the overlying water and 3–5 mm into the mat matrix. Reduced oxygen concentrations below the photosynthetic region were indicative of heterotrophic metabolism in the mat matrix. At the highest mean velocity (43.6 cm s^{-1}), no oxygen peak was apparent in the plateau area, and the oxygen peak was reduced in the depression (Fig. 8C and F). In both plateau and depression areas, oxygen peaks and oxygen penetration depths (OPD) decreased with increasing mean velocity (Table 2).

[31] During dark periods, oxygen entered the mat from the overlying, oxygenated water column, and oxygen saturation within the mat decreased with depth below the surface (Fig. 9). At low mean velocities, the convex shape of the oxygen saturation profile indicated diffusive transport of oxygen. At the highest mean velocity, the oxygen profile at one plateau location indicated advective oxygen transport to a depth of approximately 4 mm into the mat (Fig. 9C).

Discussion

[32] Sessile aquatic organisms can modify their hydrodynamic environment in ways that enhance their survival and growth (e.g., Friedrichs et al. 2000; Coco et al. 2006). Most studies of hydrodynamic modifications have concerned organisms that form porous structures such as mussel beds and macrophyte canopies. Studies of these structures have been facilitated by a well-developed theoretical framework for flow in porous media (Finnigan 2000; Lowe et al. 2008). The hydrodynamic effects of denser structures such as microbial and algal mats have received less attention, although these are the dominant biota in many benthic environments. From a fluid mechanics perspective, *D. geminata* mats and comparable structures are fibrous, compressible media with rough surfaces (relative to flow depth), low porosity, and anisotropic permeability (Jackson and James 1986). Semiempirical and theoretical models are available for flow in fibrous media (James and Davis 2001), but they are not well developed for compressible structures such as dense algal mats. Models that are appropriate for dense algal mats attached to porous cobble beds (i.e., coupled fibrous and porous media) pose a further challenge. Empirical studies such as the experiments reported here are needed to construct and test such models.

[33] The first hypothesis we tested was that *D. geminata*-covered cobbles reduce form-induced stresses, turbulent shear stress, turbulent energy, and wake turbulence, relative to bare cobble beds. These modifications would serve to reduce the risk of mat detachment. Results of ADV and PTV measurements indicated that *D. geminata* mats reduce wake turbulence and form-induced stresses, and the energy of large turbulent eddies relative to the bare cobble bed. However, turbulent and total shear stress were greater above *D. geminata* mats than bare cobbles, and u_* was consistently higher at *D. geminata* mat surfaces than at the bare cobbles beneath those mats. In addition, structures on *D. geminata* mats (e.g., plateaus, depressions, and streamers) introduced biological roughness at millimeter-to-centimeter scales scales that was not present on the bare

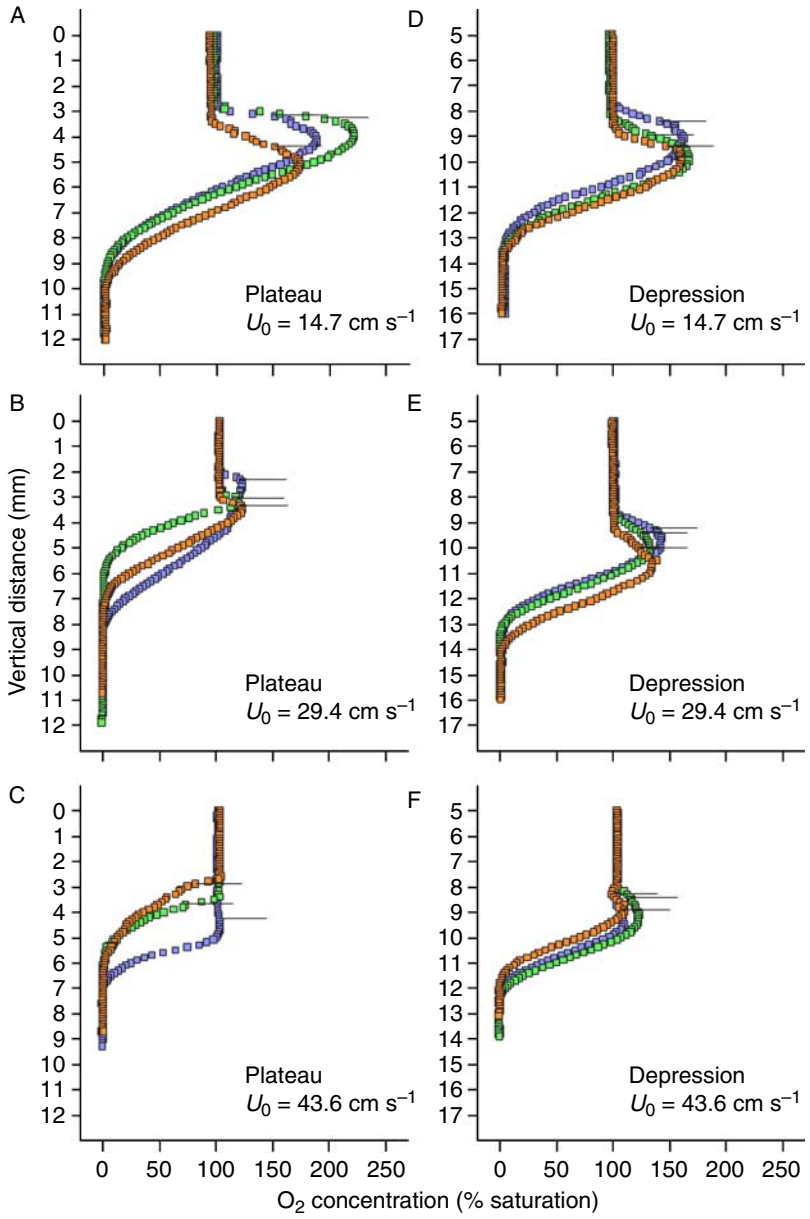

Fig. 8 Vertical profiles of dissolved oxygen saturation measured with an oxygen microsensor above and within a plateau (A–C) and a depression (D–F) on a *D. geminata* mat, at three mean velocities, under illuminated conditions. Profiles extended from a fixed position above the mat; differences in ordinates correspond to different distances from the fixed position to the mat surface. Symbols indicate replicate profiles at each plateau and depression. Dashed lines indicate mat surfaces. The mat surface could not be located precisely at the highest mean velocity.

cobble bed and that produced additional turbulent shear over the mats. The increase in friction factor values when *D. geminata* mats were present indicates that the net effect of hydraulic modifications by *D. geminata* is increased drag.

[34] Whereas *D. geminata* mats attached to cobbles experience greater drag forces than cobbles alone, the PTV data suggest a compensatory effect of the mats. For the bare cobble bed, maximum partial (2D) K was greatest in the wake regions behind cobbles and immediately above the cobble-bed surface. The zone of maximum K was shifted upward by several centimeters when *D. geminata* mats were present, which suggests that dynamic forces were reduced at mat surfaces. In addition, the autospectral analyses indicated that large, near-bed turbulent structures were reduced in energy over *D. geminata* mats in comparison to cobbles. The general reduction in near-bed turbulence may result from viscous dissipation of turbulent kinetic energy by the mats. Comparable effects have been reported for bryophyte mats and tree canopies (e.g., Nikora et al. 1998; Mammarella and Jensen 2008).

[35] The second hypothesis we tested was that high friction associated with flow through densely interwoven *D. geminata* stalks reduces advective transport within mats, which can in turn enhance nutrient retention. Measurements of solute transport supported the hypothesis. *D. geminata* mats are effective viscous dissipaters, strongly reducing or eliminating shear-driven flow just beneath mat surfaces. Under low-to-moderate shear velocities ($u_* \leq 4.2$ cm s^{-1}), diffusion was the dominant transport mode in the mats to within 1 mm of the mat surface. Under higher shear velocities, mats began to fluidize and advection dominated in the upper 4–5 mm, but diffusion still dominated below this zone. Whereas microelectrode measurements only extended 6 mm into the 1–5-cm-thick mats, we can assume that diffusion-dominated transport extended to mat bases. The dissolved oxygen profiles were consistent

Table 2 Dissolved oxygen peaks and oxygen penetration depths (OPD) in *Didymosphenia geminata* mats. Values are means ± 1 SD, $n = 3$.

			Dissolved oxygen peak (% saturation)		OPD (mm)	
Light treatment	Flow (L s^{-1})	U_0 (cm s^{-1})	Plateau	Depression	Plateau	Depression
Light	14	14.7	195 ± 24	164 ± 3	6.1 ± 0.1	4.9 ± 0.3
Light	27	29.4	122 ± 2	138 ± 5	4.5 ± 1.4	4.6 ± 0.2
Light	40	43.6	104 ± 1	114 ± 8	3.0 ± 0.7	3.7 ± 0.4
Dark	14	14.7	—	—	1.7 ± 0.4	1.3 ± 0.2
Dark	27	29.4	—	—	2.0 ± 0.5	1.1 ± 0.1
Dark	40	43.6	—	—	—	—

with our interpretation of shifting dominance in transport modes. At low-to-moderate flow rates, photosynthetic oxygen from illuminated *D. geminata* cells diffused downward into the mat matrix and upward into a boundary layer above the mat. Negative relationships between mean velocity and oxygen penetration depth (OPD) and peak oxygen concentration indicate that photosynthetic oxygen was flushed from the *D. geminata* mat at high velocities. The same process occurs in microbial mats, biofilms, and microphytobenthos (Jørgensen and Des Marais 1990; Berninger and Huettel 1997). Both OPD and peak oxygen concentration decreased with increasing velocity more rapidly in a "plateau" region compared with a depression, which suggests that there is less flushing and greater solute retention in depressions compared with the surrounding mat surface. This spatial pattern results from the interaction of streamflow and the rough mat surface, which yields higher pressures on exposed surfaces compared with depressions (Jørgensen and Des Marais 1990).

[36] The predominance of diffusive transport in the surficial portions of *D. geminata* mats at low flows and advective transport at high flows suggests a mechanism by which *D. geminata* cells acquire nutrients from different sources. At low flows, dissolved nutrients derived from organic matter in mat matrices and underlying substrata diffuse toward the *D. geminata* cells at mat surfaces, with minimal advective losses. As flows increase, advective losses from mats also increase but are offset by increased nutrient mass transport from the overlying water to mat surfaces. Positive relationships between mass transport and near-bed velocity have been reported for many benthic autotrophs, including dense algal mats and turfs (Larned and Atkinson 1997; Carpenter and Williams 2007). *D. geminata* may acquire dissolved nutrients from both mat matrices and the overlying water column, with the proportion of nutrients supplied from each source varying with flow conditions. A similar strategy for nutrient acquisition has been demonstrated for *Dictyosphaeria cavernosa* (Forsskål) Børgesen, a mat-forming green alga. *D. cavernosa* mats can sustain net growth when supplied with nutrients from the oligotrophic water column in high-energy environments but require diffusive inputs of nutrients from organic matter in mat matrices in low-energy environments (Larned and Atkinson 1997). Numerous cases have been reported of mat-forming autotrophs "trapping" dissolved nutrients released from POM within and below mats (e.g., Larned 1998; Tyler et al. 2003); this appears to be a common strategy for nutrient acquisition in oligotrophic, low-energy environments.

[37] Current evidence for a dual nutrient-source strategy in *D. geminata* is limited to our observations of flow-dependent changes in transport processes within mats, low ambient nutrient-concentrations in *D. geminata*-dominated rivers, and large quantities of POM within and beneath *D. geminata* mats (Flöder and Kilroy 2009; Whitton et al. 2009). More compelling evidence would include high concentrations of dissolved nutrients and/or high rates of POM remineralization in mat matrices, and demonstration of mass transport-limited nutrient uptake. Oxygen depletion within *D. geminata* mat matrices (Figs. 8 and 9) suggests that heterotrophic

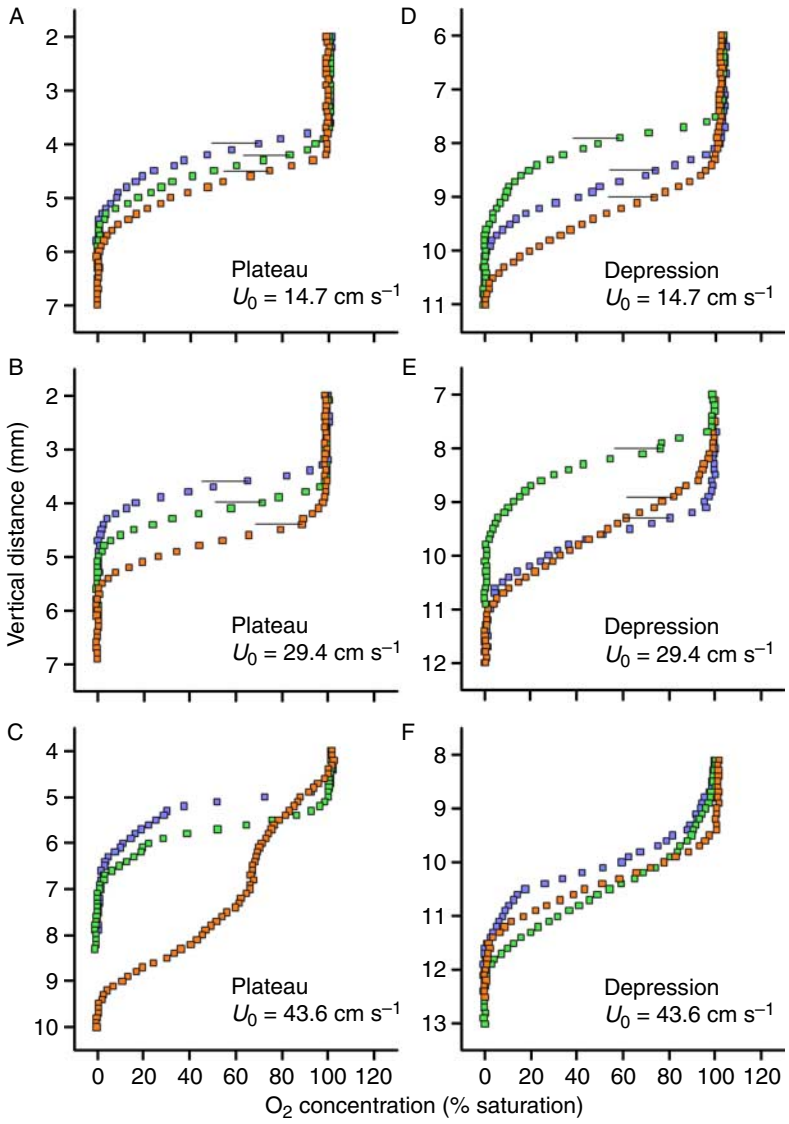

Fig. 9 Vertical profiles of dissolved oxygen saturation above and within a plateau (A–C) and a depression (D–F) on a *Didymosphenia geminata* mat, in darkness. Profiles extended from a fixed position above the mat; differences in ordinates correspond to different distances from the fixed position to the mat surface. Symbols indicate replicate profiles at each plateau and depression. Dashed lines indicate mat surfaces. The mat surface could not be precisely located at the highest mean velocity (C and F).

organisms are abundant, and these organisms may enhance POM remineralization.

[38] We propose that modifications of near-bed flow structure by *D. geminata* mats are part of a flow-organism feedback system that allows *D. geminata* to persist in rivers. Flow-organism feedback systems consist of responses by organisms to flow conditions (e.g., changes in organism shape, inclination, or motion), flow modifications induced by the organisms, subsequent responses by the organisms to the modified flow, and so forth (Coco et al. 2006). We measured flow modifications by *D. geminata* but not responses by *D. geminata* to flow conditions. However, we can predict likely responses based on previous studies. Many lotic macrophytes and algae undergo reversible reconfiguration in response to changing near-bed flow conditions (Holbrook et al. 1991; Sand-Jensen 2003; O'Hare et al. 2007). Reversible reconfiguration refers to progressive bending and streamlining of stalks, leaves, filaments, and blades with increasing near-bed velocity and straightening and expansion as near-bed velocities decrease. This process reduces viscous and form drag at high flows and enhances turbulent mass transport at low flows. In the case of *D. geminata*, we predict that entire mats compress and expand in response to flow fluctuations; these responses are typical of flexible, dense aggregations of macrophytes and algae (Holbrook et al. 1991; Abdelrhman 2007). The general pattern of decreasing $\langle U \rangle / U_0$ with increasing U_0 in our study (Fig. 3B) may reflect compression of *D. geminata* mats at high flows (and, consequently, greater cross-sectional flow area). A rigorous evaluation of flow-organism feedback in *D. geminata* will require analyses of more reconfiguration responses, and consideration of the trade-offs caused by reconfiguration between drag reduction and nutrient acquisition.

Significance to Aquatic Environments

[39] Benthic autotrophs living in swift, oligotrophic rivers must have morphologies that balance the conflicting requirements for minimal drag and maximal nutrient supply. There are numerous combinations of growth forms (e.g., size, shape, physical orientation) and structural properties (e.g., stiffness, tensile strength) that

achieve this balance, as indicated by the diversity of morphologies that occur in rivers. Specific combinations of growth forms and structural properties contribute to the "survival strategies" of benthic autotrophs (Denny 2006). These strategies can be assessed from two different perspectives: responses of organisms to their environment, or modifications of the environment by organisms. The first perspective corresponds to studies of phenotypic plasticity and mechanical behaviors such as reconfiguration and flapping (e.g., O'Hare et al. 2007). The second corresponds to studies of flow modifications by organisms (e.g., Nikora et al. 1998). In our analysis of *D. geminata*, we focused on flow modification as a survival strategy. Dense mats like those created by *D. geminata* are particularly well adapted to life in high-energy, oligotrophic rivers. These mats can reduce the risk of detachment by reducing near-bed form-induced stress and turbulent kinetic energy. In addition, *D. geminata* may enhance the turbulent delivery of nutrients from the water column to mat surfaces and the retention and recycling of nutrients within mats. The hydrodynamic effects of *D. geminata* may represent a common strategy for benthic autotrophs in high-energy, oligotrophic environments. Many other algae, cyanobacteria, and bryophytes form dense mats (Larned 1998; Suren et al. 2000; Stal 2000), and their hydrodynamic effects may be similar to those of *D. geminata*. It is important to note that the survival and proliferation of *D. geminata* does not depend solely on modification of hydrodynamic conditions; it is likely that reconfiguration and morphological plasticity of the alga also have important roles.

Acknowledgments We thank Vladimir Nikora (University of Aberdeen), Philip Gillibrand (National Institute of Water and Atmospheric Research), and two anonymous referees for thoughtful reviews of the manuscript. Funding was provided by the New Zealand Foundation for Research, Science and Technology, Water Allocation Programme (contract no. C01X0308). Roger Nokes (University of Canterbury) provided equipment and software for the PTV measurements.

Appendix

Table A1 Hydraulic conditions during particle tracking velocimetry (PTV), acoustic Doppler velocimetry (ADV), and whole-channel measurements with *Didymosphenia geminata* mats in place and after mats were removed (bare cobbles). Experiment numbers refer to collection date. *H*: flow depth. U_0: cross-sectional mean velocity. u_*: shear velocity. z_0: roughness length. *d*: displacement height. *Re*: Reynolds number. *Fr*: Froude number. S: water surface slope. *f*: Darcy-Weisbach friction factor.

Treatment	Experiment	Flow ($L\,s^{-1}$)	*H* (cm)	U_0 ($cm\,s^{-1}$)	u_* from logarithmic equation ($cm\,s^{-1}$)	u_* from turbulent shear stress ($cm\,s^{-1}$)	z_0 (cm)	*d* (cm)	*Re*	*Fr*
PTV measurements										
D. geminata mats	2	13.5	15.3	14.7	1.7	1.7	0.5	−12.6	20,400	0.120
Bare cobbles	2	13.5	16.7	13.5	1.2	1.2	0.6	−16.7	20,500	0.110
ADV measurements										
D. geminata mats	1	14	15.8	14.7	1.4	1.2	—	—	21,100	0.118
D. geminata mats	1	27	15.3	29.4	2.2	2.1	—	—	40,900	0.240
D. geminata mats	1	40	15.3	43.6	4.4	4.6	—	—	60,600	0.356
D. geminata mats	2	20	13.9	23.9	2.2	2.2	—	—	30,200	0.205
D. geminata mats	2	35	14.0	41.8	4.2	3.8	—	—	53,200	0.357
D. geminata mats	2	50	14.1	59.1	—	4.4	—	—	75,800	0.503
Bare cobbles	1	14	17.8	13.0	1.2	1.0	—	—	21,100	0.118
Bare cobbles	1	27	17.3	26.0	1.9	2.0	—	—	40,900	0.200
Bare cobbles	1	40	17.3	38.5	3.8	3.1	—	—	60,600	0.296
Bare cobbles	2	35	16.7	35.0	3.9	3.0	—	—	53,100	0.273

Whole-channel measurements									
Treatment	**Experiment**	**Flow (L s^{-1})**	***H* (cm)**	***U*$_0$ (cm s^{-1})**	***u*$_*$ (cm s^{-1})**	***Re***	***Fr***	***S***	***f***
D. geminata mats	2	8.9	9	16.5	3.1	13,500	0.175	0.0014	0.28
D. geminata mats	2	13.6	9	25.2	4.9	20,600	0.268	0.0035	0.30
D. geminata mats	2	18	9	33.3	6.2	27,300	0.355	0.0057	0.28
D. geminata mats	2	21.6	9	40.0	7.5	32,700	0.426	0.0083	0.28
D. geminata mats	2	15.8	9	29.3	5.6	23,900	0.311	0.0046	0.29
D. geminata mats	2	12	9	22.2	4.2	18,200	0.237	0.0026	0.29
D. geminata mats	2	7	9	13.0	2.2	10,600	0.138	0.0007	0.22
D. geminata mats	2	9.1	0.14	10.8	1.1	13,800	0.092	0.0001	0.09
D. geminata mats	2	12	0.14	14.3	1.6	18,200	0.122	0.0003	0.10
D. geminata mats	2	15	0.14	17.9	2.3	22,700	0.152	0.0006	0.13
D. geminata mats	2	18	0.14	21.4	3.2	27,300	0.183	0.0011	0.18
D. geminata mats	2	21	0.14	25.0	3.8	31,800	0.213	0.0015	0.18
D. geminata mats	2	24.2	0.14	28.8	4.4	36,700	0.246	0.0021	0.19
D. geminata mats	2	27	0.14	32.1	5.0	40,900	0.274	0.0026	0.19
D. geminata mats	2	30	0.14	35.7	5.6	45,500	0.305	0.0033	0.20
D. geminata mats	2	35	0.14	41.7	6.8	53,000	0.356	0.0050	0.22
D. geminata mats	2	40	0.14	47.6	7.9	60,600	0.406	0.0067	0.22
D. geminata mats	2	45	0.14	53.6	9.2	68,200	0.457	0.0090	0.24
Bare cobbles	2	9	0.117	12.8	1.9	13,600	0.120	0.0004	0.17
Bare cobbles	2	12.3	0.117	17.5	2.8	18,600	0.164	0.0010	0.21
Bare cobbles	2	14.8	0.117	21.1	3.4	22,400	0.197	0.0014	0.21
Bare cobbles	2	18.7	0.117	26.6	4.0	28,300	0.249	0.0019	0.18
Bare cobbles	2	21.2	0.117	30.2	4.8	32,100	0.282	0.0028	0.20
Bare cobbles	2	23.9	0.117	34.0	5.5	36,200	0.318	0.0036	0.21
Bare cobbles	2	27	0.117	38.5	6.2	40,900	0.359	0.0046	0.20
Bare cobbles	2	30.2	0.117	43.0	7.0	45,800	0.402	0.0060	0.21
Bare cobbles	2	9.1	0.167	9.1	1.2	13,800	0.071	0.0001	0.14
Bare cobbles	2	11.9	0.167	11.9	1.7	18,000	0.093	0.0003	0.17
Bare cobbles	2	14.9	0.167	14.9	2.4	22,600	0.116	0.0006	0.21
Bare cobbles	2	18	0.167	18.0	2.7	27,300	0.140	0.0007	0.18
Bare cobbles	2	21	0.167	21.0	3.0	31,800	0.164	0.0008	0.16
Bare cobbles	2	24	0.167	24.0	3.4	36,400	0.187	0.0011	0.16
Bare cobbles	2	27	0.167	26.9	4.0	40,900	0.211	0.0015	0.18
Bare cobbles	2	30.3	0.167	30.2	4.5	45,900	0.236	0.0019	0.18
Bare cobbles	2	35.1	0.167	35.0	5.3	53,200	0.274	0.0026	0.18
Bare cobbles	2	40.3	0.167	40.2	6.0	61,100	0.314	0.0035	0.18
Bare cobbles	2	45.1	0.167	45.0	6.8	68,300	0.352	0.0044	0.18

ASLO Advancing the science of limnology and oceanography
DUKE UNIVERSITY PRESS

Table A2 Hydraulic, chemical, and light conditions during oxygen and hydrogen microelectrode profiling above and within *Didymosphenia geminata* mats. The hydrogen microelectrode was used to measure normalized transport rates. Experiment number refers to collection date. Depression and plateau refer to topographic features on mat surfaces used for oxygen measurements. Mat 1 and Mat 2 refer to two mats located at opposite ends of the flume that were used for measuring transport rates. U_0: cross-sectional mean velocity. u_*: shear velocity.

Experiment	Flow (L s^{-1})	U_0 (cm s^{-1})	u_* (cm s^{-1})	Location	Electrical conductivity (μS cm^{-1})	Temperature (°C)	pH	Photosynthetically active radiation (μmol quanta m^{-2} s^{-1})
Oxygen microelectrode measurements								
1	14	14.7	1.4	Depression	132.1	17.7	7.6	120
1	14	14.7	1.4	Depression	132.6	18.8	7.6	120
1	14	14.7	1.4	Depression	132.9	17.8	7.6	120
1	14	14.7	1.4	Depression	136.8	19.8	7.7	0
1	14	14.7	1.4	Depression	136.5	19.5	7.7	0
1	14	14.7	1.4	Depression	136.4	19.5	7.7	0
1	14	14.7	1.4	Plateau	132.1	17.6	7.6	120
1	14	14.7	1.4	Plateau	131.7	17.6	7.6	120
1	14	14.7	1.4	Plateau	131.7	18.4	7.6	120
1	14	14.7	1.4	Plateau	136.2	19.4	7.7	0
1	14	14.7	1.4	Plateau	136.0	19.4	7.7	0
1	14	14.7	1.4	Plateau	135.8	19.4	7.7	0
1	27	29.4	2.2	Depression	133.2	17.9	7.6	120
1	27	29.4	2.2	Depression	133.6	19.3	7.6	120
1	27	29.4	2.2	Depression	133.7	18.4	7.6	120
1	27	29.4	2.2	Depression	135.6	19.6	7.6	0
1	27	29.4	2.2	Depression	135.6	19.2	7.6	0
1	27	29.4	2.2	Depression	135.5	19.2	7.6	0
1	27	29.4	2.2	Plateau	134.0	18.3	7.6	120
1	27	29.4	2.2	Plateau	134.3	18.4	7.7	120
1	27	29.4	2.2	Plateau	134.4	18.5	7.7	120
1	27	29.4	2.2	Plateau	135.7	19.3	7.6	0
1	27	29.4	2.2	Plateau	135.6	19.2	7.6	0
1	27	29.4	2.2	Plateau	135.7	19.2	7.6	0
1	40	43.6	4.4	Depression	135.9	19.2	7.7	120
1	40	43.6	4.4	Depression	136.2	19.3	7.7	120
1	40	43.6	4.4	Depression	136.6	19.5	7.7	120
1	40	43.6	4.4	Depression	135.6	19.2	7.6	0
1	40	43.6	4.4	Depression	135.8	19.2	7.6	0
1	40	43.6	4.4	Depression	136.1	19.4	7.6	0
1	40	43.6	4.4	Plateau	134.7	19.4	7.7	120
1	40	43.6	4.4	Plateau	135.1	18.8	7.7	120
1	40	43.6	4.4	Plateau	135.5	18.9	7.7	120
1	40	43.6	4.4	Plateau	136.3	19.4	7.6	0
1	40	43.6	4.4	Plateau	136.5	19.5	7.6	0
1	40	43.6	4.4	Plateau	136.8	19.5	7.6	0
Hydrogen microelectrode measurements								
2	0	0.0	0.0	Mat 1	—	—	—	120
2	0	0.0	0.0	Mat 1	—	—	—	120
2	0	0.0	0.0	Mat 1	—	—	—	120
2	13.5	14.7	1.7	Mat 1	—	—	—	120
2	20	23.9	2.2	Mat 1	127.8	20.9	7.4	120
2	35	41.8	4.2	Mat 1	128.0	20.9	7.4	120
2	50	59.1	ND	Mat 1	128.8	21.5	7.5	120
2	0	0.0	0.0	Mat 2	130.1	21.9	7.5	120
2	0	0.0	0.0	Mat 2	130.2	22.2	7.5	120
2	13.5	14.7	1.7	Mat 2	130.4	22.0	7.4	120
2	20	23.9	2.2	Mat 2	130.5	21.9	7.4	120
2	35	41.8	4.2	Mat 2	130.6	22.3	7.5	120

ASLO Advancing the science of limnology and oceanography
DUKE UNIVERSITY PRESS

References

Abdelrhman, M. A. 2007. Modelling coupling between eelgrass *Zostera marina* and water flow. Mar. Ecol. Prog. Ser. **338**: 81–96, doi:10.3354/meps338081.

Bendat, J. S., and A. G. Piersol. 2000. Random Data: Analysis and Measurement Procedures. 3rd ed. Wiley.

Berninger, U. G., and M. Huettel. 1997. Impact of flow on oxygen dynamics in photosynthetically active sediments. Aquat. Microb. Ecol. **12**: 291–300, doi:10.3354/ame012291.

Biggs, B. J. F., D. G. Goring, and V. I. Nikora. 1998. Subsidy and stress responses of stream periphyton to gradients in water velocity as a function of community growth form. J. Phycol. **34**: 598–607, doi:10.1046/j.1529-8817.1998.340598.x.

Biggs, B. J. F., V. I. Nikora, and T. H. Snelder. 2005. Linking scales of flow variability to lotic ecosystem structure and function. River Res. Appl. **21**: 283–298, doi:10.1002/rra.847.

Blanco, S., and L. Ector. 2009. Distribution, ecology and nuisance effects of the freshwater invasive diatom *Didymosphenia geminata* (Lyngbye) M. Schmidt: A literature review. Nova Hedwigia. **88**: 347–422, doi:10.1127/0029-5035/2009/0088-0347.

Carpenter, R. C., and S. L. Williams. 2007. Mass transfer limitation of photosynthesis of coral reef algal turfs. Mar. Biol. **151**: 435–450, doi:10.1007/s00227-006-0465-3.

Cline, A. K., and R. L. Renka. 1984. A storage-efficient method for computation of a Thiessen triangulation. Rocky Mountain J. Math. **14**: 119–140, doi:10.1216/RMJ-1984-14-1-119.

Coco, G., S. F. Thrush, M. O. Green, and J. E. Hewitt. 2006. The role of feedbacks between bivalve density, flow, and suspended sediment concentration on patch stable states. Ecology. **87**: 2862–2870, doi:10.1890/0012-9658(2006)87[2862:FBBDFA]2.0.CO;2.

De Beer, D., and M. Kühl. 2001. Interfacial microbial mats and biofilms. Pp. 374–394. *In* B. P. Boudreau and B. B. Jørgensen [eds.], The Benthic Boundary Layer. Oxford University Press.

Denny, M. W. 2006. Ocean waves, nearshore ecology, and natural selection. Aquat. Ecol. **40**: 439–461, doi:10.1007/s10452-004-5409-8.

Dodds, W. K. 2003. The role of periphyton in phosphorus retention in shallow freshwater aquatic ecosystems. J. Phycol. **39**: 840–849, doi:10.1046/j.1529-8817.2003.02081.x.

Finnigan, J. 2000. Turbulence in plant canopies. Annu. Rev. Fluid Mech. **32**: 519–571, doi:10.1146/annurev.fluid.32.1.519.

Flöder, S., and C. Kilroy. 2009. *Didymosphenia geminata* (Protista, Bacillariophyceae) invasion, resistance of native periphyton communities, and implications for dispersal and management. Biodivers. Conserv. **18**: 3809–3824, doi:10.1007/s10531-009-9681-8.

Friedrichs, M., G. Graf, and B. Springer. 2000. Skimming flow induced over a simulated polychaete tube lawn at low population densities. Mar. Ecol. Prog. Ser. **192**: 219–228, doi:10.3354/meps192219.

Holbrook, N. M., M. W. Denny, and M. A. R. Koehl. 1991. Intertidal "trees": Consequences of aggregation on the mechanical and photosynthetic properties of sea-palms *Postelsia palmaeformis* Ruprecht. J. Exp. Mar. Biol. Ecol. **146**: 39–67, doi:10.1016/0022-0981(91)90254-T.

Jackson, G. W., and D. F. James. 1986. The permeability of fibrous porous media. Can. J. Chem. Eng. **64**: 364–374, doi:10.1002/cjce.5450640302.

James, D. F., and A. M. Davis. 2001. Flow at the interface of a model fibrous porous medium. J. Fluid Mech. **426**: 47–72, doi:10.1017/S0022112000002160.

Jørgensen, B. B., and D. Des Marais. 1990. The diffusive boundary layer of sediments: oxygen microgradients over a microbial mat. Limnol. Oceanogr. **35**: 1343–1355, doi:10.4319/lo.1990.35.6.1343.

Kirkwood, A. E., T. Shea, L. J. Jackson, and E. McCauley. 2007. *Didymosphenia geminata* in two Alberta headwater rivers: An emerging invasive species that challenges conventional views on algal bloom development. Can. J. Fish. Aquat. Sci. **64**: 1703–1709, doi:10.1139/F07-152.

Kilroy, C., T. H. Snelder, O. Floerl, C. C. Vieglais, and K. L. Dey. 2008. A rapid technique for assessing the suitability of areas for invasive species applied to New Zealand's rivers. Divers. Distrib. **14**: 262–272, doi:10.1111/j.1472-4642.2007.00406.x.

Kilroy, C., S. T. Larned, and B. J. F. Biggs. 2009. The non-indigenous diatom Didymosphenia geminata alters benthic communities in New Zealand rivers. Freshwater Biol. **54**: 1990–2002, doi:10.1111/j.1365-2427.2009.02247.x.

Kumar, S., S. A. Spaulding, T. J. Stohlgren, K. Hermann, T. Schmidt, and L. Bahls. 2009. Potential habitat distribution for the freshwater diatom *Didymosphenia geminata* in the continental US. Front. Ecol. Environ. **7**: 415–420, doi:10.1890/080054.

Larned, S. T. 1998. Nitrogen- versus phosphorus-limited growth and sources of nutrients for coral reef macroalgae. Mar. Biol. **132**: 409–421, doi:10.1007/s002270050407.

Larned, S. T., and M. J. Atkinson. 1997. Effects of water velocity on NH_4 and PO_4 uptake and nutrient-limited growth in the macroalga *Dictyosphaeria cavernosa*. Mar. Ecol.: Prog. Ser. **157**: 295–302, doi:10.3354/meps157295.

Larned, S. T., V. I. Nikora, and B. J. F. Biggs. 2004. Mass transfer-limited nitrogen and phosphorus uptake by stream periphyton: A conceptual model and experimental evidence. Limnol. Oceanogr. **49**: 1992–2000, doi:10.4319/lo.2004.49.6.1992.

Lowe, R. J., U. Shavit, J. L. Falter, J. R. Koseff, and S. G. Monismith. 2008. Modeling flow in coral communities with and without waves: A synthesis of porous media and canopy flow approaches. Limnol. Oceanogr. **53**: 2668–2680, doi:10.4319/lo.2008.53.6.2668.

Mammarella, I. E. D., and N. O. Jensen. 2008. Turbulence spectra, shear stress and turbulent kinetic energy budgets above two beech forest sites in Denmark. Tellus B Chem. Phys. Meteorol. **60**: 179–187, doi:10.1111/j.1600-0889.2007.00326.x.

ASLO Advancing the science of limnology and oceanography DUKE UNIVERSITY PRESS

Miller, M. P., D. M. McKnight, J. D. Cullis, A. Greene, K. Vietti, and D. Liptzin. 2009. Factors controlling streambed coverage of Didymosphenia geminata in two regulated streams in the Colorado Front Range. Hydrobiologia. **630**: 207–218, doi:10.1007/s10750-009-9793-x.

Nikora, V. I., D. G. Goring, and B. J. F. Biggs. 1997. On stream periphyton-turbulence interactions. N. Z. J. Mar. Freshwater Res. **31**: 435–448, doi:10.1080/00288330.1997.9516777.

Nikora, V. I., A. M. Suren, S. L. R. Brown, and B. J. F. Biggs. 1998. The effects of the moss *Fissidens rigidulus* (Fissidentaceae: Musci) on near-bed flow structure in an experimental cobble bed flume. Limnol. Oceanogr. **43**: 1321–1331, doi:10.4319/lo.1998.43.6.1321.

Nikora, V., D. Goring, I. McEwan, and G. Griffiths. 2001. Spatially averaged open-channel flow over rough bed. J. Hydraul. Eng. **127**: 123–133, doi:10.1061/(ASCE)0733-9429(2001)127:2(123).

Nokes, R. I. 2007. FluidStream 7.00—System Theory and Design. Department of Civil Engineering, University of Canterbury, Christchurch, New Zealand.

O'Hare, M., K. A. Hutchinson, and R. T. Clarke. 2007. The drag and reconfiguration experienced by five macrophytes from a lowland river. Aquat. Bot. **86**: 253–259, doi:10.1016/j.aquabot.2006.11.004.

Plew, D., G. Cooper, and F. Callaghan. 2008. Turbulence-induced forces in a freshwater macrophyte canopy. Water Resour. Res. **44**: W02414, doi:10.1029/2007WR006064.

Puijalon, S., G. Bornette, and P. Sagnes. 2005. Adaptations to increasing hydraulic stress: Morphology, hydrodynamics and fitness of two higher aquatic plant species. J. Exp. Bot. **56**: 777–786, doi:10.1093/jxb/eri063.

Raven, J. A. 1992. How benthic macroalgae cope with flowing freshwater: Resource acquisition and retention. J. Phycol. **28**: 133–146, doi:10.1111/j.0022-3646.1992.00133.x.

Revsbech, N. P., L. P. Nielsen, and N. B. Ramsing. 1998. A novel microsensor for determination of apparent diffusivity in sediments. Limnol. Oceanogr. **43**: 986–992, doi:10.4319/lo.1998.43.5.0986.

Rice, S. K., and P. H. Schuepp. 1995. On the ecological and evolutionary significance of branch and leaf morphology in aquatic *Sphagnum* (Sphagnaceae). Am. J. Bot. **82**: 833–846, doi:10.2307/2445969.

Sand-Jensen, K. 2003. Drag and reconfiguration of freshwater macrophytes. Freshwater Biol. **48**: 271–283, doi:10.1046/j.1365-2427.2003.00998.x.

Schutten, J., and A. J. Davy. 2000. Predicting the hydraulic forces on submerged macrophytes from current velocity biomass and morphology. Oecologia. **123**: 445–452, doi:10.1007/s004420000348.

Stal, L. J. 2000. Cyanobacterial mats and stromatolites. Pp. 61–120. *In* B. A. Whitton and M. Potts [eds.], The Ecology of Cyanobacteria. Kluwer Academic Publishers.

Steinman, A. D., P. J. Mulholland, and W. R. Hill. 1992. Functional responses associated with growth form in stream algae. J. N. Am. Benthol. Soc. **11**: 229–243, doi:10.2307/1467388.

Stevens, C. L., C. L. Hurd, and P. E. Isachsen. 2003. Modelling of diffusion boundary layers in subtidal macroalgal canopies: The response to waves and currents. Aquat. Sci. **65**: 81–91, doi:10.1007/s000270300007.

Suren, A. M., G. M. Smart, R. A. Smith, and S. L. R. Brown. 2000. Drag coefficients of stream bryophytes: experimental determinations and ecological significance. Freshwater Biol. **45**: 309–317, doi:10.1111/j.1365-2427.2000.00621.x.

Tyler, A. C., K. J. McGlathery, and I. C. Anderson. 2003. Benthic algae control sediment-water column fluxes of organic and inorganic nitrogen compounds in a temperate lagoon. Limnol. Oceanogr. **48**: 2125–2137, doi:10.4319/lo.2003.48.6.2125.

Vitt, D. H., and J. M. Glime. 1984. The structural adaptations of aquatic Musci. Lindbergia. **10**: 95–110.

Vopel, K., and I. Hawes. 2006. Photosynthetic performance of benthic microbial mats in Lake Hoare, Antarctica. Limnol. Oceanogr. **51**: 1801–1812, doi:10.4319/lo.2006.51.4.1801.

Whitton, B. A., N. T. W. Ellwood, and B. Kawecki. 2009. Biology of the freshwater diatom Didymosphenia: A review. Hydrobiologia. **630**: 1–37, doi:10.1007/s10750-009-9753-5.

Received: 7 April 2010
Amended: 9 August 2010
Accepted: 2 November 2010